解度が低いため、DMSO等の有機溶媒共存下での操作となった。

種々の条件で実験を進めたが、結晶が溶解するケースが多くみられたため、タンパク質架橋剤（クロスリンク）を利用して、結晶の状態を維持することも試みた。また、溶解度の低さを補うため、化合物を粉末状態のままで結晶化溶液に添加することも試みた。これによって、結晶に色づきがみられ、化合物が結晶相に移行していることが観測された。

これらの結果を踏まえ、SPring8/BL38B1等で回折測定を行った。得られたデータはタンパク質単体の結晶からの回折強度に比べると若干分解能が落ちるものの構造決定には支障のないものであった。しかしながら、現時点では化合物に相当する電子密度は得られていない。

D．考察

通常、タンパク質の結晶化は水溶液の条件で行われるために、水溶媒に溶解度の低い化合物は十分な量を溶液中に分散させることができず、占有率（結晶中で対象となる原子分子がその部位を占めている割合）の高い複合体作成は難しくなる。特に、親和性の弱い化合物の場合は、複合体結晶形成のために、数十から数百ミリモル/L程度の溶液を使うことも一般的であり、希薄な条件での成功率は高くない。

今回、この問題を解決するために、粉末状態の化合物を直接結晶化溶液等に添加してみた。この結果、結晶の色づきがみられ、タンパク質分子と何らかの結合を起こしていることが示唆される。溶液中の化合物分子数が高く維持できなくとも、結晶相にゆっくりと移行するものと想定される。この手法に、Crosslinkなどによる結晶の補強法等を組み合わせることで結晶自体の破壊を抑制できれば、今後のスクリーニングにも有効だと考えている。

しかしながら、結晶構造自体は現時点では得られていない。これまでの研究でNMRでは相互作用が確認できていることに加え、最近Benzamidineなどの非常に単純な構造を持つ低分子がRasに結合している様子が明らかとなったこと(Maurer et al. PNAS 109,5299(2012))を考え合わせると、解析を試みる候補分子についても、それらのフラグメントについて検討するなどの対応が必要となるであろう。

E．結論

薬剤候補化合物との複合体結晶解析に必要な手法の確立を進め、溶解度の低い試料についても結晶試料調製が可能であることが示唆された。

これまでのところ、結合構造は検出できていないが、上記の方法を活用し、今後は解析を試みる分子の検討を進める。特に最新の*in silico*ドッキングスクリーニングと生化学的活性検証試験で新たな母核候補が10種類ほど得られている。これらは分子サイズが比較的小さく300ほどの分子量で、水溶性もある程度担保されているため、これらについて複合体の構造決定を行う予定である。構造決定ができれば、複合体の構造情報に基づく化合物の構造最適化を行う予定である。

G．研究発表

1．論文発表

○Matsumoto K, Shima F, Muraoka S, Araki M, Hu L, Ijiri Y, Hirai R, Liao J, Yoshioka T, Kumasaka T, Yamamoto M, Tamura A, Kataoka T.
Critical roles of interactions among switch I-preceding residues and between switch II and its neighboring alpha-helix in conformational dynamics of the GTP-bound Ras family small GTPases.
J. Biol. Chem. 2011 Apr 29; 286(17):15403-12.

2．学会発表

なし。

H．知的財産権の出願・登録状況

1．特許取得

①名称：微小試料用キャピラリー
発明者：熊坂崇、牧野正知、桑本いづみ、山本雅貴
出願番号：特願2012-18603
出願日：平成24年1月31日

②名称：MUTANT RAS POLYPEPTYDE CRYSTAL
発明者：Tohru Kataoka, Fumi Shima, Atsuo Tamura, Takashi Kumasaka
出願番号：US13/383835（特願2009-165717）
出願日：平成24年1月12日（優先日：平成21年7月14日）

2．実用新案登録

なし。

3．その他

なし。

III. 研究成果の刊行に関する一覧表

研究成果の刊行に関する一覧表レイアウト

書籍

著者氏名	論文タイトル名	書籍全体の編集者名	書　籍　名	出版社名	出版地	出版年	ページ
なし							

雑誌

発表者氏名	論文タイトル名	発表誌名	巻号	ページ	出版年
Araki M, Shima F, Yoshikawa Y, Muraoka S, Ijiri Y, Nagahara Y, Shirono T, Kataoka T, Tamura A.	Solution Structure of the State 1 Conformer of GTP-bound H-Ras Protein and Distinct Dynamic Properties between the State 1 and State 2 Conformers.	*J. Biol. Chem.*	286	39644-39653	2011
Matsumoto K, Shima F, Muraoka S, Araki M, Hu L, Ijiri Y, Hirai R, Liao J, Yoshioka T, Kumasaka T, Yamamoto M, Tamura A, Kataoka T.	Critical roles of interactions among switch I-preceding residues and between switch II and its neighboring alpha-helix in conformational dynamics of the GTP-bound Ras family small GTPases.	*J. Biol. Chem.*	286	15403-15412	2011

Ⅳ．研究成果の刊行物・別刷

THE JOURNAL OF BIOLOGICAL CHEMISTRY VOL. 286, NO. 45, pp. 39644–39653, November 11, 2011

Solution Structure of the State 1 Conformer of GTP-bound H-Ras Protein and Distinct Dynamic Properties between the State 1 and State 2 Conformers*[S]

Received for publication, February 1, 2011, and in revised form, August 25, 2011 Published, JBC Papers in Press, September 19, 2011, DOI 10.1074/jbc.M111.227074

Mitsugu Araki[‡], Fumi Shima[§], Yoko Yoshikawa[§], Shin Muraoka[§], Yuichi Ijiri[§], Yuka Nagahara[‡], Tomoya Shirono[§], Tohru Kataoka[§1], and Atsuo Tamura[‡2]

From the [‡]Department of Chemistry, Kobe University Graduate School of Science, 1-1 Rokkodai, Nada-ku, Kobe 657-8501 and the [§]Division of Molecular Biology, Department of Biochemistry and Molecular Biology, Kobe University Graduate School of Medicine, 7-5-1 Kusunoki-cho, Chuo-ku, Kobe 650-0017, Japan

Ras small GTPases undergo dynamic equilibrium of two interconverting conformations, state 1 and state 2, in the GTP-bound forms, where state 2 is recognized by effectors, whereas physiological functions of state 1 have been unknown. Limited information, such as static crystal structures and ^{31}P NMR spectra, was available for the study of the conformational dynamics. Here we determine the solution structure and dynamics of state 1 by multidimensional heteronuclear NMR analysis of an H-RasT35S mutant in complex with guanosine 5′-(β, γ-imido)-triphosphate (GppNHp). The state 1 structure shows that the switch I loop fluctuates extensively compared with that in state 2 or H-Ras-GDP. Also, backbone ^{1}H,^{15}N signals for state 2 are identified, and their dynamics are studied by utilizing a complex with c-Raf-1. Furthermore, the signals for almost all the residues of H-Ras·GppNHp are identified by measurement at low temperature, and the signals for multiple residues are found split into two peaks corresponding to the signals for state 1 and state 2. Intriguingly, these residues are located not only in the switch regions and their neighbors but also in the rigidly structured regions, suggesting that global structural rearrangements occur during the state interconversion. The backbone dynamics of each state show that the switch loops in state 1 are dynamically mobile on the picosecond to nanosecond time scale, and these mobilities are significantly reduced in state 2. These results suggest that multiconformations existing in state 1 are mostly deselected upon the transition toward state 2 induced by the effector binding.

Small GTPases H-Ras, K-Ras, and N-Ras, collectively called Ras, are the products of the *ras* proto-oncogenes and function as molecular switches by cycling between the GTP-bound active and the GDP-bound inactive forms in intracellular signaling pathways controlling proliferation, differentiation, and apoptosis of cells. GTP hydrolysis on Ras is markedly stimulated by GTPase-activating proteins, whereas conversion from the GDP-bound form to the GTP-bound form is promoted by guanine nucleotide exchange factors (1, 2). Ras comprise the Ras family of small GTPases together with a number of its relatives including Rap1, Rap2, R-Ras, R-Ras2/TCL, M-Ras/R-Ras3, RalA, RalB, etc. (3). Structural studies of Ras showed that structural differences between the GDP- and GTP-bound forms universally exist in two flexible regions, called switch I (residues 32–38 in H-Ras) and switch II (residues 60–75 in H-Ras) (1). GTP-sensitive orientation of the switch regions enables Ras to interact with their effectors such as Raf kinases and phosphoinositide 3-kinases (2).

Recent ^{31}P NMR studies suggested that H-Ras in the nucleoside triphosphate form exists in equilibrium between two kinds of conformational states, state 1 and state 2, around the phosphate groups of GTP or its non-hydrolyzable analogues, GppNHp[3] and GTPγS, bound to the protein (4–6). This conformational heterogeneity has been commonly observed in a number of Ras homologues (7, 8). Because binding to the various effectors, such as c-Raf-1, shifted the equilibrium toward state 2 (5, 9), state 1 and state 2 were regarded as the "inactive" and "active" conformations, respectively. The x-ray structures of H-Ras·GppNHp by itself or in complex with its effectors revealed the state 2 conformation in which the switch I and switch II regions are fixed by hydrogen bonds of the backbone amides of Thr-35 and Gly-60, respectively, with the γ-phosphate oxygen atoms of the nucleoside triphosphate (1, 10–12). On the other hand, x-ray structures corresponding to state 1 were recently determined by using H-Ras mutants, H-RasT35S·GppNHp (9, 13) and H-RasG60A·GppNHp (14), or M-Ras·GppNHp (15), all of which predominantly adopted state 1, whereas that of H-Ras·GppNHp has remained unsolved. In these state 1 structures, Thr-45 (corresponding to Thr-35 in H-Ras) of M-Ras and Ser-35 of H-RasT35S are not capable of

* This work was supported by Grants-in-aid for Scientific Research in Priority Areas 17014061 and 18057014 and Global COE Program A08 from the Ministry of Education, Science, Sports, and Culture of Japan and by Grant for the Program for Promotion of Fundamental Studies of Health Sciences 06-3 from the National Institute of Biomedical Innovation.

[S] The on-line version of this article (available at http://www.jbc.org) contains supplemental Figs. 1–3.

The atomic coordinates and structure factors (code 2LCF) have been deposited in the Protein Data Bank, Research Collaboratory for Structural Bioinformatics, Rutgers University, New Brunswick, NJ (http://www.rcsb.org/).

[1] To whom correspondence may be addressed. E-mail: kataoka@people.kobe-u.ac.jp.

[2] To whom correspondence may be addressed. E-mail: tamuatsu@kobe-u.ac.jp.

[3] The abbreviations used are: GppNHp, guanosine 5′-(β, γ-imido)triphosphate; GTPγS, guanosine 5′-3-*O*-(thio)triphosphate; Sos, Son of sevenless; HSQC, heteronuclear single-quantum coherence; RBD, Ras binding domain; TOCSY, total correlated spectroscopy; r.m.s.d., root-mean-square deviation; NOESY, nuclear overhauser effect spectroscopy.

interacting with the guanine nucleotide and magnesium ion, causing marked deviation of the switch I loop from the nucleotide (13, 15). This structural feature of state 1 results in greater exposure of the nucleotide to the solvent and allows faster association and dissociation of GTP compared with state 2 (7). A similar switch I loop deviation was observed in the conformation of nucleotide-free H-Ras in complex with Sos, a guanine nucleotide exchange factor for Ras. In the structure of the H-Ras-Sos complex, the helical hairpin segment of Sos opens wide the nucleotide-binding site, causing deviation of the switch I loop of H-Ras further away from this site (16). The results suggested that state 1 might play a role in the guanine nucleotide cycle involving guanine nucleotide exchange factors, although its function remained to be clarified (14, 17). So far studies on the state transition of the GTP-bound Ras have been based on static crystal structures or ^{31}P NMR spectra, which are in principle unsuitable for studying the dynamic aspects of conformational transition.

Heteronuclear NMR spectroscopy is the most suitable technique to examine detailed conformational dynamics of proteins in solution. Nevertheless, structural studies on the GTP-bound Ras using this technique have been hampered by chemical exchange processes at intermediate rates on the NMR time scale that result in broadening or even disappearance of the resonance signals (18–20). Although the solution structure of RalB·GppNHp in state 1 was recently determined by this technique, backbone amide resonances were not observed for several residues in the switch regions. In the case of H-Ras in complex with GppNHp or GTPγS, backbone amide ^{1}H,^{15}N HSQC cross-peaks underwent extreme broadening for most of the residues in the P-loop (residues 10–17) and switch I and switch II regions (19). Also, in the physiological GTP-bound form, the cross-peaks from these regions were two to four times broader than the normal ones (19), although they dominantly existed as state 2 as revealed by ^{31}P NMR (4, 5). These results imply that the exchange processes are an intrinsic property of H-Ras in the nucleoside triphosphate form. The analysis of ^{15}N spin relaxation relaxation-compensated Carr-Purcell-Meiboom-Gill measurements showed that the exchange processes involve a major part of the H-Ras structure (21). However, conformational species representing the exchange processes have not been characterized.

In this study, we report successful assignments of the backbone resonances for state 1 and state 2 by ^{1}H and ^{15}N NMR analysis of H-RasT35S·GppNHp and H-Ras·GppNHp in complex with c-Raf-1 RBD, respectively. Moreover, the backbone resonances for almost all the residues of H-Ras·GppNHp are successfully identified by measurement at low temperature. Comparison of these resonance data proves that the chemical exchange process observed in ^{1}H and ^{15}N NMR of H-Ras·GppNHp corresponds to the interconversion between state 1 and state 2. Also, analysis of the backbone dynamics by measuring ^{15}N relaxation times and heteronuclear NOEs reveals a significant difference in rapid internal motions of the switch regions between state 1 and state 2. Furthermore, the solution structure of state 1 is solved with H-RasT35S·GppNHp for the first time. It shows unique conformations of the switch regions, some of which are very similar to those of the nucleotide-free form found in the H-Ras-Sos complex. These structural features characteristic of state 1 will be discussed in relation to results of H-Ras/Sos binding experiments.

EXPERIMENTAL PROCEDURES

Protein Expression and Purification—Residues 1–166 of human H-Ras and H-RasT35S were expressed as fusions with glutathione *S*-transferase in *Escherichia coli* using pGEX-6P-1 vector (GE Healthcare). M9 minimal media containing $^{15}NH_4Cl$ and [^{13}C]glucose/$^{15}NH_4Cl$ were used to express the uniformly ^{15}N-labeled and ^{15}N/^{13}C-labeled proteins, respectively. Proteins were immobilized on glutathione-agarose and eluted by cleavage with PreScission protease (GE Healthcare). After further purification by ion exchange chromatography to a final purity of >95% as measured by SDS-PAGE, they were loaded with GppNHp (Sigma). Human c-Raf-1 RBD consisting of residues 51–130 was purified as described (7).

NMR Spectroscopy—Each protein sample was concentrated and dissolved in a buffer containing 25 mM sodium phosphate, pH 6.8, 150 mM NaCl, and 10 mM $MgCl_2$ in 90% $^{1}H_2O$ and 10% $^{2}H_2O$ using a centrifugal filter unit. For the 100% $^{2}H_2O$ samples, the protein solutions were incubated at 34 °C for 4 days after buffer displacement and filtration with a filter (0.2 μm pore size). Protein concentrations were determined by absorbance measurements as described (22). NMR measurements were performed on a Bruker DMX-750 spectrometer on protein samples of 1.0–2.0 mM concentration at 25 °C unless stated otherwise. The following spectra were acquired on ^{13}C,^{15}N-labeled H-RasT35S·GppNHp: triple-resonance spectra of HNCA, HN(CO)CA, CBCA(CO)NH, HNCO, HBHA(CO)NH, HBHANH, and H(CC)(CO)NH in addition to ^{13}C-separated TOCSY-HSQC, NOESY-HSQC, HCCH-TOCSY, and HCCH-COSY (23). Triple-resonance spectra of HNCA, HN(CO)CA, HNCO, and HBHA(CO)NH were acquired on ^{13}C,^{15}N-labeled H-Ras·GppNHp. ^{15}N-Separated TOCSY-HSQC and NOESY-HSQC spectra were recorded on ^{15}N-labeled H-Ras·GppNHp and H-RasT35S·GppNHp. Two-dimensional homonuclear ^{1}H NOESY spectra were recorded on the unlabeled proteins. Mixing times of all NOESY experiments were 100 ms. The backbone $^{1}H_N$ and ^{15}N resonances of H-Ras·GppNHp alone were assigned at 5 °C by analyzing the ^{1}H,^{15}N HSQC and ^{15}N-separated NOESY-HSQC spectra at 5, 15, and 25 °C. In the presence of c-Raf-1 RBD, the $^{1}H_N$ and ^{15}N resonances at 5 °C were identified by pursuing the traces of the individual cross-peaks in the ^{1}H,^{15}N HSQC spectra at 5, 15, and 25 °C. All chemical shifts were referenced to 3-(trimethylsilyl) propionate sodium salt.

Backbone Dynamics—All experiments were carried out at 25 °C on 1.5 mM ^{15}N-labeled H-RasT35S·GppNHp. ^{15}N T_1, T_2, and heteronuclear NOE measurements were performed using the pulse sequence previously reported (24). T_1 experiments were recorded with time delays of 0.01, 0.05, 0.1, 0.2, 0.3, 0.4, 0.6, 0.8, and 1.0 s, in which ^{1}H 180° pulses were applied every 5 ms to eliminate the effects of cross-correlation between ^{1}H,^{15}N dipolar and ^{15}N chemical shift anisotropy relaxation mechanisms (25). T_2 experiments were recorded with time delays of 0.0170, 0.0339, 0.0509, 0.0678, 0.0848, 0.1018, and 0.1187 s in which ^{15}N 180° pulses at a field strength of 3.1 kHz were applied

every 0.9 ms, and ^{1}H 180° pulses were applied every 8.4 ms to suppress cross-correlated relaxation. The intensity decays were fitted using an equation $I(t) = I_0 \exp(-t/T_{1,2})$. ^{1}H,^{15}N steady-state heteronuclear NOE measurements were carried out by recording a pair of spectra with and without proton saturation using a total recycle delay of 3.2 s in which proton saturation of 3 s was achieved by applying 120° proton pulses every 5 ms. The NOE values were analyzed by calculating the peak height ratios obtained from reference and saturated experiments (I_{sat}/I_{ref}). The series of experiments was also performed on a mixture containing 1.5 mM ^{15}N-labeled H-Ras·GppNHp and 1.8 mM unlabeled c-Raf-1 RBD in which state 2 was predominantly populated (5).

Structure Calculations of H-RasT35S·GppNHp—In the N-terminal sequence (GPLGSD) corresponding to remainder of the cleavage site by PreScission protease, intense NMR signals indicated that this region is unstructured with high mobility. Interproton distance restraints were obtained from the ^{13}C-separated NOESY-HSQC, ^{15}N-separated NOESY-HSQC, and two-dimensional homonuclear ^{1}H NOESY spectra recorded at 25 °C. Standard pseudo atom distances were used when they were needed. Structures were calculated by using the program CYANA 2.1 (26) and CNS 1.2 (27). A large number of ambiguous NOE peaks were identified by iterative calculations using structures computed from unambiguously assigned peaks, whereas 568 NOEs were excluded from the calculation because of overlapping with other signals or difficulty to remove ambiguity. A total of 3116 meaningful NOE upper distance restraints were finally obtained by CYANA, including 1021 long range distances. Backbone torsion angle restraints ϕ and ψ were estimated from the C_α, C_β, C′, H_N, N, and H_α chemical shifts using the program TALOS (28). The error values were set to twice the standard deviation of the TALOS prediction. The GppNHp nucleotide was modeled by adding distance restraints to coordinate the Mg^{2+} ion to three water molecules, the $O^{2\beta}$ and $O^{2\gamma}$ of GppNHp and the side-chain oxygen atom of Ser-17 as shown in the x-ray structure of H-RasT35S·GppNHp (13). A total of 100 structures was generated by using CYANA, then the 20 structures with the lowest target function that had no NOE violations more than 0.2 Å and no dihedral angle violations more than 5° were refined using CNS. The lowest energy structures finally obtained were selected to represent three-dimensional structure and analyzed using PROCHECK-NMR software (29). The atomic coordinates have been deposited in the Protein Data Bank (PDB code 2LCF).

RESULTS

Assignments of the Backbone Resonances for State 1 and State 2—In the two-dimensional ^{1}H,^{15}N HSQC spectrum for H-Ras·GppNHp, it was previously reported that the backbone amide ^{1}H,^{15}N cross-peaks could not be detected for residues 10–13 in the P-loop, 31–39 in or near switch I, and 57–64 and 71 in or near switch II (19). Its temperature and magnetic field dependencies indicated that these regions undergo the structural conversion between two or more stable conformations, named as "polysterism"(19). The structural basis for this polysterism has been unknown even though it looks in parallel with the interconversion between state 1 and state 2 observed in the ^{31}P NMR spectrum of H-Ras·GppNHp (5). On the other hand, H-RasT35S·GppNHp exists almost exclusively in state 1 as revealed by its ^{31}P NMR spectrum, showing that each phosphate resonance, especially that of the γ-phosphate, yields a single peak equivalent to the state 1 peak of H-Ras·GppNHp (9). Hence, we investigated this mutant protein by heteronuclear NMR spectroscopy. In contrast to the case of H-Ras·GppNHp, complete assignments of the backbone ^{1}H, ^{13}C, and ^{15}N resonances were achieved for all the 166 residues of H-RasT35S·GppNHp by analysis of the seven triple-resonance NMR spectra (see "Experimental Procedures" for details). The assigned resonances were expected to represent the chemical shift positions for state 1.

^{31}P NMR studies showed that binding to c-Raf-1 RBD shifts the conformational equilibrium of H-Ras·GppNHp toward state 2 (5, 9). In the ^{1}H,^{15}N HSQC spectra of H-Ras·GppNHp, the addition of c-Raf-1 RBD generated cross-peaks corresponding to the P-loop and the switch regions, which were missing in its free form (19). We thus attempted to assign the complete backbone resonances of ^{13}C,^{15}N -labeled H-Ras·GppNHp in complex with unlabeled c-Raf-1 RBD. However, the backbone ^1H_N and ^{15}N resonances, which are correlated with the intra-residue and sequential $^{13}C_\alpha$ resonances, were observed for only 134 residues through the HNCA and HN(CO)CA spectra because the sensitivity of the triple-resonance three-dimensional NMR spectra became notably lower in the presence of c-Raf-1 RBD. Therefore, we assigned all the backbone ^1H_N and ^{15}N resonances excluding Glu-31 by combining the analysis of ^{15}N-separated NOESY-HSQC spectrum, which gives especially intense cross-peaks correlating ^1H_N of one residue to $^1H_\alpha$ and $^1H_\beta$ of the intra- and preceding residues. Nonetheless, ambiguities inherent in the assignments for the residues 30–36 could not be removed as NOEs or $^{13}C_\alpha$,^1H_N correlations were detected partially for these residues concomitantly with broadening of the ^{1}H,^{15}N HSQC cross-peaks even in the presence of an equimolar amount of c-Raf-1 RBD. In a similar manner, we assigned all the backbone ^1H_N and ^{15}N resonances of ^{13}C,^{15}N-labeled H-RasT35S·GppNHp in complex with unlabeled c-Raf-1 RBD, except for Glu-31, Asp-33, Ser-35, and Ile-36. The assigned resonances for H-Ras·GppNHp and H-RasT35S·GppNHp, bound to c-Raf-1 RBD, were almost identical excluding the residue 35 and its adjacent region, and expected to represent the chemical shift positions for state 2.

Assignment of the Backbone Resonances of H-Ras·GppNHp—We assigned the backbone ^{1}H, ^{13}C, and ^{15}N resonances for most of the 166 residues of H-Ras·GppNHp through analysis of the triple-resonance NMR spectra by referring to the previous assignments (19). We failed to detect the ^{1}H,^{15}N cross-peaks for most of the residues in the P-loop and the switch regions when the measurements were done at 25 °C as reported (19). However, the spectrum measured at 5 °C yielded 20 additional cross-peaks, some of which are indicated by *solid boxes* in Fig. 1. When these new peaks were compared with the state 1 and state 2 peaks, measured at 5 °C on H-RasT35S·GppNHp and the H-Ras·GppNHp·c-Raf-1 RBD complex, respectively, most of them were found overlapped with state 1 or state 2 peaks of the residues whose signals were undetectable upon the measurement of H-Ras·GppNHp at 25 °C. For example, two

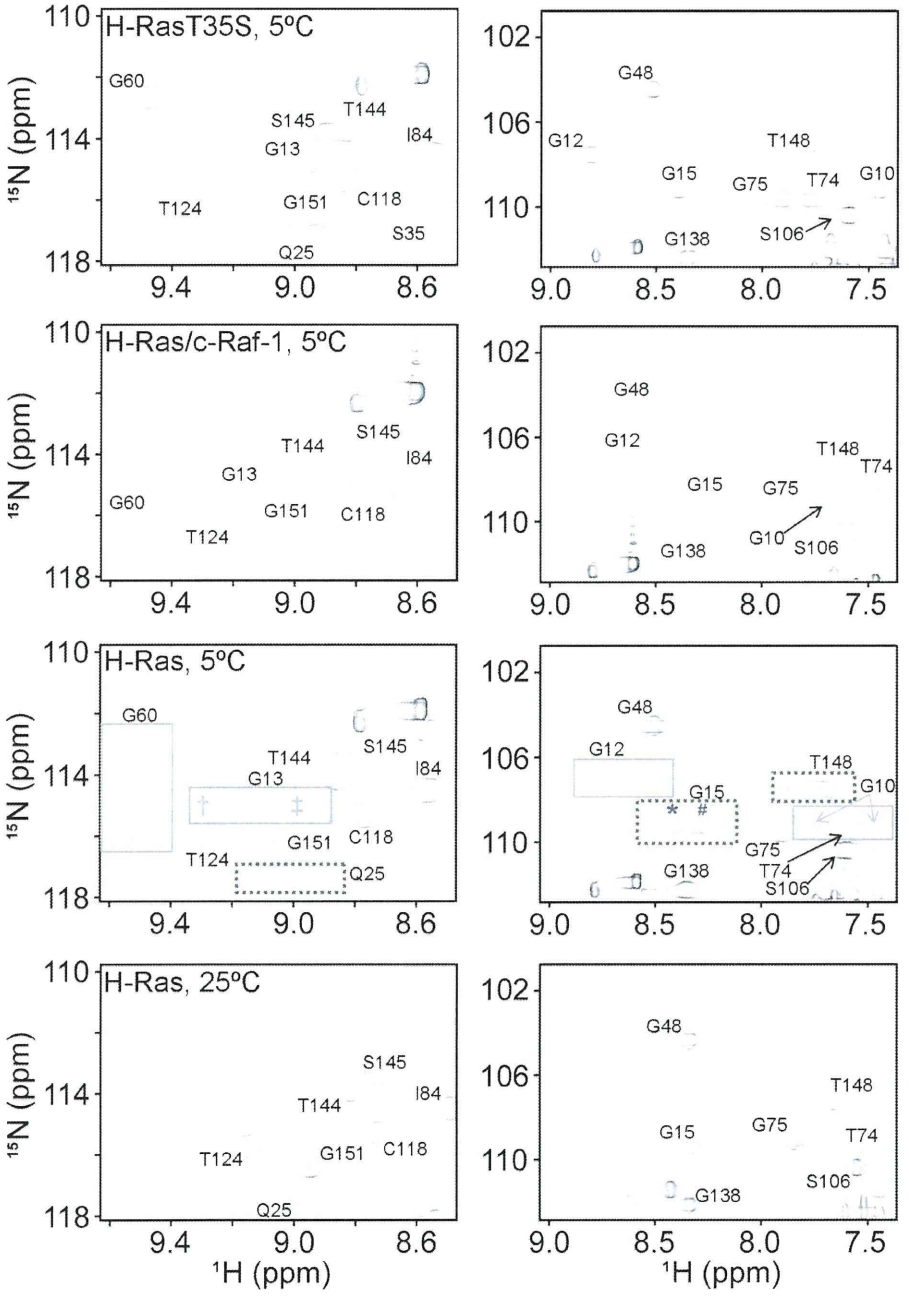

FIGURE 1. **Contour plots of the two different regions (*right* and *left*) of ^{1}H,^{15}N HSQC spectra for H-RasT35S·GppNHp (5 °C), H-Ras·GppNHp in complex with c-Raf-1 RBD (5 °C), H-Ras·GppNHp (5 °C), and H-Ras·GppNHp (25 °C).** The *dotted* and *solid boxes* highlight the splitting cross-peaks for the residues that exhibited single and undetectable peaks, respectively, at 25 °C. ‡ and † represent the cross-peaks for Gly-13 corresponding to state 1 and state 2, respectively. * and # represent the cross-peaks for Gly-15 corresponding to state 1 and state 2, respectively.

new peaks of H-Ras·GppNHp indicated by ‡ and † in Fig. 1 coincided with the state 1 (H-RasT35S·GppNHp) and state 2 (H-Ras·GppNHp·c-Raf-1 RBD complex) peaks of Gly13, respectively. Similarly, two separate peaks corresponding to both state 1 and state 2 were identified for Gly-10, Gly-12, and Gly-60 (Fig. 1). For most of the residues in the switch regions, one or both of the peaks for the two states were overlapped with other peaks, preventing accurate identification. Furthermore, the measurement at 5 °C caused splitting of several cross-peaks as indicated by *boxes drawn by dotted lines* in Fig. 1. In most of these cases, one of the split peaks overlapped with the state 1 peak, whereas the other was located near the state 2 peak. For example, Gly-15 gave a single peak at 25 °C, whereas it was split into two peaks at 5 °C as indicated by * and # in Fig. 1, which coincided with the state 1 and state 2 peaks, respectively. The new results obtained for the H-Ras·GppNHp spectra at 5 °C could be ascribable to the difference in the static magnetic field strength, *i.e.* 17.6T compared with 9.4 (14.1)T in the previous

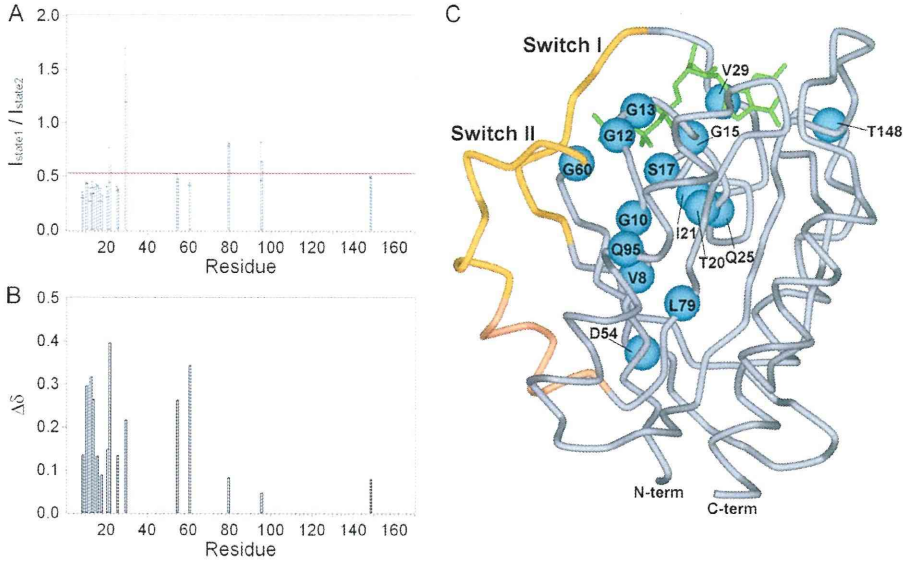

FIGURE 2. **Characterization of the residues sensitive to the state transition.** *A*, shown are plots of the integrated intensity ratio of a pair of split cross-peaks (I_{state1}/I_{state2}) for the backbone amide $^{1}H,^{15}N$ HSQC spectrum of H-Ras·GppNHp at 5 °C against the amino acid sequence. In the case of the residues that exhibited splitting into more than three cross-peaks, we selected and compared two of them for each residue according to the peak positions in the spectrum of H-RasT35S·GppNHp as state 1 and those in the spectrum of H-Ras·GppNHp in complex with c-Raf-1 RBD as state 2, respectively. The mean value is indicated by a *red line*. *B*, plots of chemical shift differences of the split cross-peaks against the amino acid sequence are shown. The difference was calculated by using the function $\Delta\delta = [(\Delta\delta_{1H})^2 + (0.1\Delta\delta_{15N})^2]^{0.5}$. *C*, shown are the locations of the residues with high dynamic property shown in the molecular model of H-Ras·GppNHp (5P21). The protein backbone and GppNHp are represented by a *gray backbone tube* and *green sticks*, respectively. The switch I and switch II loops are colored in *orange*. The nitrogen atoms in the backbone amides exhibiting peak splitting are depicted as *blue spheres*. The models were generated by the program ViewerLite (Accelrys, Inc. San Diego, CA).

work (19). Intensity ratios and chemical shift differences of the split peaks unambiguously assigned were plotted against the amino acid sequence (Fig. 2, *A* and *B*). Most of the intensity ratios (I_{state1}/I_{state2}) were distributed in the range of 0.3–0.8 with the mean value of 0.53, which was close to the equilibrium constant between state 1 and state 2 ($1/K_{12}$) with the value of 0.6, derived from the ^{31}P NMR (8). In the tertiary structure of H-Ras·GppNHp, the residues exhibiting the peak splitting are distributed in the P-loop, switch II, and the rigidly structured regions (Fig. 2*C*).

Solution Structure of H-RasT35S·GppNHp and Conformational Assessment of Its Switch Regions—The chemical shift resonances were assigned for all the side chains of H-RasT35S·GppNHp, except for the ^{1}H and ^{13}C resonances derived from γ-ϵ positions of Lys-16, ϵ-ζ positions of Phe-82, and γ-ϵ positions of Lys-117. The H1 and H8 chemical shifts for the purine ring and the H1′-H3′ shifts for the ribose ring of GppNHp were assigned from two-dimensional ^{1}H NOESY and TOCSY spectra. A total of 5636 NOEs were translated by CYANA into meaningful 3116 upper distance restraints. The final structural calculation was performed with these distance restraints in addition to 114 ϕ and 116 ψ backbone dihedral angle restraints (Table 1). The overall NMR structure of H-RasT35S·GppNHp was well defined excluding pre-switch I (residues 28–31), switch I, and switch II regions, with the r.m.s.d. value of 0.48 ± 0.05 Å (Fig. 3*A* and Table 1). The structure was consistent with typical guanine nucleotide-binding proteins, which consist of a six-stranded β-sheet (β1–6) surrounded by five α-helices (α1–5) (1) (Fig. 3*B*). A profile of residual dipolar couplings of the rigidly structured regions in H-RasT35S·GppNHp provided a good correlation between

TABLE 1
Structural statistics for the 20 lowest energy structures of H-RasT35S·GppNHp

Ramachandran analysis was evaluated by using the program PROCHECK (29).

Number of distance restraints	
Total	3116
Intraresidue	812
Short range ($\|i-j\|$ = 1 residue)	750
Medium range ($\|i-j\|$ = 2–4 residues)	533
Long range ($\|i-j\|$ >4 residues)	1021
Number of torsion angle restraints, ϕ / ψ	114/116
r.m.s.d. from experimental restraints	
Distance constraints (Å)	0.0069 ± 0.0007
Torsion angle constraints (°)	0.026 ± 0.008
r.m.s.d. from ideal covalent geometry	
Bond lengths (Å)	0.0011 ± 0.0001
Bond angles (°)	0.34 ± 0.05
Impropers (°)	0.32 ± 0.19
r.m.s.d. from the mean structure (Å)	
Backbone atoms (residues 1–27, 39–59, 76–166)	0.48 ± 0.05
All heavy atoms (residues 1–27, 39–59, 76–166)	0.89 ± 0.05
Backbone atoms (residues 1–166)	0.87 ± 0.12
All heavy atoms (residues 1–166)	1.31 ± 0.12
Ramachandran analysis	
Most favored regions (%)	81.2
Additional allowed regions (%)	16.9
Generously allowed regions (%)	1.5
Disallowed regions (%)	0.4

experimentally measured and theoretical residual dipolar couplings calculated from the mean structure of the 20 structures we determined, supporting validation of the structural model encompassing these regions (supplemental Fig. 1). On the other hand, residues 28–38 and 59–64 constituting the switch I and switch II loops, respectively, were poorly defined (Fig. 3*A*). Also, multiple residues in the switch loops exhibit residual dipolar coupling outliers with smaller experimental values, suggesting flexibilities of these loop regions (supplemental Fig. 1).

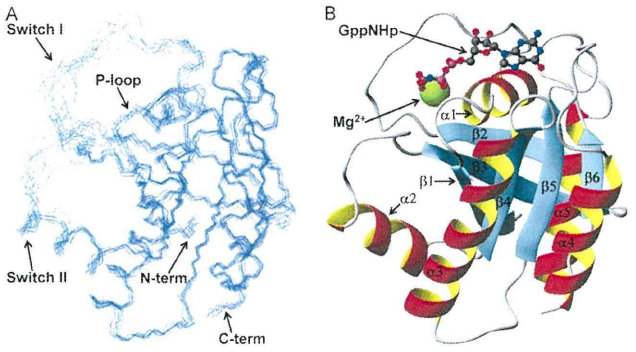

FIGURE 3. **NMR structure of H-RasT35S·GppNHp.** *A*, shown are backbone traces of the 20 lowest energy structures. *B*, shown is a ribbon diagram of the overall mean structure. The Mg^{2+} ion (*green*) and nucleotide (*gray*, carbon; *blue*, nitrogen; *magenta*, phosphorus; *red*, oxygen) are shown by Corey-Pauling-Koltun and *ball-and-stick models*, respectively. The models were generated by the program MOLMOL (41).

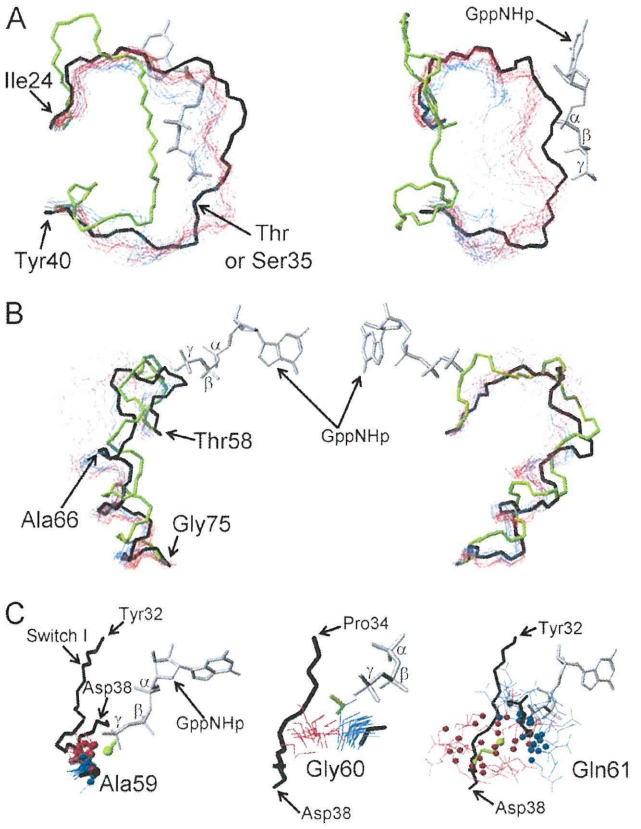

FIGURE 4. **Comparison of the NMR and the crystal structures in the two switch regions of H-Ras.** The NMR structures of H-RasT35S·GppNHp (PDB ID 2LCF, *blue*) and H-Ras-GDP (PDB ID 1CRP, *brown*) (30), the crystal structures of H-Ras·GppNHp (PDB ID 5P21, *black*) (10), and the nucleotide-free form of H-Ras (PDB ID 1BKD, *green*) (16) are shown. GppNHp in the crystal structures of H-Ras·GppNHp was represented by *thick lines in gray*. The models were generated by fitting to minimize root mean square deviation from the first structure of H-RasT35S·GppNHp for the residues 1–31, 39–59, and 76–166. *A*, shown is superimposition of the backbone structures for the pre-switch I and the switch I residues 24–40 in two orientations. *B*, shown is superimposition of the backbone structures for the switch II and its flanking residues 58–75 in two orientations. *C*, shown are detailed structures for the residues 59–61. The side chains and the C_α atoms of Ala-59 (*left panel*) and Gln-61 (*right panel*) are shown by *lines* and *spheres*, respectively. C-N-C_α bonds of Gly-60 (*middle panel*) are shown by *lines*. The side chains and the C-N-C_α bond of H-Ras·GppNHp and the nucleotide-free H-Ras were depicted as *thick lines*.

In Fig. 4, the backbone structure of the two switch regions of H-RasT35S·GppNHp (state 1) (*blue*) was compared with those of the x-ray structures of H-Ras·GppNHp (state 2, PDB code 5P21 (10)) (*black*) and the nucleotide-free form of H-Ras (PDB code 1BKD (16)) (*green*) and of the NMR structure of H-Ras-GDP (PDB code 1CRP (30)) (*brown*). Ser-35 in switch I was located too far from the nucleotide to form a direct hydrogen bond with the γ-phosphate as observed for the corresponding residues in the state 1 structures, such as H-RasT35S·GppNHp form 1 and form 2, H-RasG60A·GppNHp, M-Ras·GppNHp, and RalB·GppNHp (13–15, 20). Intriguingly, some of the 20 switch I structures resembled that of the nucleotide-free H-Ras in complex with Sos (Fig. 4*A*), whereas one of them resembled that of H-RasGppNHp state 2. These results indicated that in solution H-RasT35S·GppNHp possesses a wide range of structural variations in switch I, the extent of which was further compared with those found on other NMR structures, H-Ras-GDP and RalB·GppNHp (state 1, PDB code 2KE5 (20)). By using CYANA, the backbone r.m.s.d. for switch I (residues 32–38) of H-RasT35S·GppNHp is calculated to be 0.89 ± 0.18 Å, which is notably larger than 0.58 ± 0.16 and 0.48 ± 0.17 Å, respectively, for the corresponding regions of H-Ras-GDP (residues 32–38) and RalB·GppNHp (residues 43–49) (Fig. 4*A*). The differences in the r.m.s.d. values could be accounted for as follows. The NOESY spectra of RalB·GppNHp gave unambiguous cross-peaks that correlated the methyl group of the Thr-46 (corresponding to Thr-35 in H-Ras) side chain to the Phe-82 ring protons and the Leu-67 side chain showing interactions between switch I and switch II (20). In the H-Ras-GDP structure, the phenol ring of Tyr-32 was located near the magnesium ion and the phenol ring of Tyr-40, which was consistent with the nearly normal values of the heteronuclear NOE, T_1, and T_2 in the residues 33–40 (30). These results indicated that the switch I regions of H-Ras-GDP and RalB·GppNHp are constrained by some non-local interactions. On the other hand, in the H-RasT35S·GppNHp structure, any long range NOEs ($|i - j| > 4$) involving the residues 30–36 could not be observed, whereas sequential and medium range NOEs including Y32C$^{\delta}$H-I36C$^{\delta}$H and D33C$^{\beta}$H-I36C$^{\gamma}$H were present. Thus, a large portion of switch I of H-RasT35S·GppNHp is stabilized only by local interactions, resulting in the markedly large r.m.s.d. value.

In contrast, the backbone r.m.s.d. values for switch II were calculated to be 0.77 ± 0.33 and 0.75 ± 0.18 Å, respectively, for H-RasT35S·GppNHp (residues 60–75) and RalB·GppNHp (residues 71–86), both of which were significantly smaller than 1.21 ± 0.23 Å for H-Ras-GDP (residues 60–75) (Fig. 4*B*). This was consistent with the presence of a small number of long range NOEs including A59C$^{\beta}$H-Y64C$^{\delta}$H, G12NH-G60C$^{\alpha}$H, and S65C$^{\alpha}$H-Q99N$^{\varepsilon}$H in the residues 59–65 of H-RasT35S·GppNHp, whereas the corresponding region of H-Ras-GDP was remarkably ill-defined due probably to lack of long range NOEs. Many of the 20 structures of H-RasT35S·GppNHp showed that the backbone amide proton of Gly-60 is not located too far to form a hydrogen bond with the γ-phosphate oxygen of GppNHp (data not shown). Moreover,

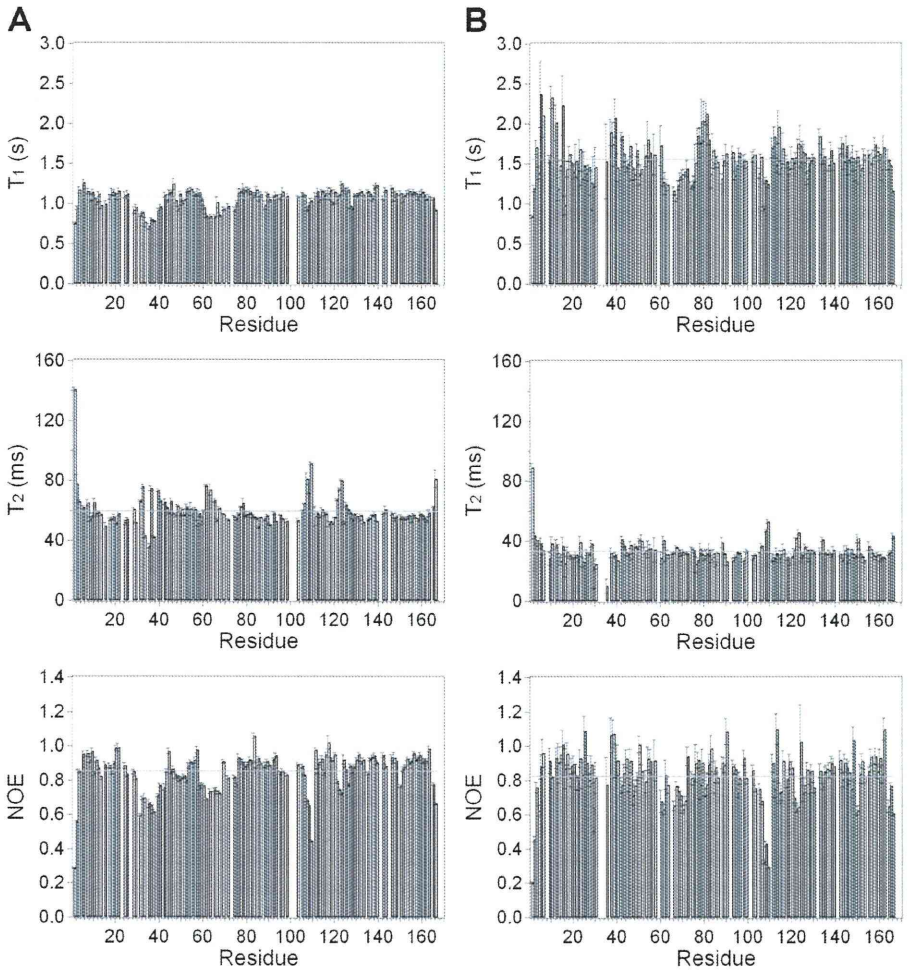

FIGURE 5. **Plots of the ^{15}N T_1, T_2, and the heteronuclear NOE for the residues in H-RasT35S·GppNHp alone (*A*) and H-Ras·GppNHp in the presence of c-Raf-1 RBD (*B*).** Mean values are indicated by *horizontal lines*.

the backbone trajectories of this residue were moderately biased and similar to the orientation of H-Ras·GppNHp state 2 (Fig. 4*C*), suggesting a high probability of forming the Gly-60-γ-phosphate hydrogen bond in the solution structure of H-RasT35S·GppNHp. This gained a strong support from the fact that the formation of the Gly-60-γ-phosphate hydrogen bond was actually observed in the x-ray structure, H-RasT35S·GppNHp form 2 (13). The results collectively indicated that switch I of H-RasT35S·GppNHp exhibits a wide range of structural variations, whereas switch II is moderately constrained by some non-local interactions including the hydrogen bond with GppNHp.

Backbone Amide Dynamics—To assess the mobility of the poorly defined loops in H-RasT35S·GppNHp more rigorously, we studied the backbone dynamics by measuring ^{15}N relaxation times and heteronuclear NOEs. For the study of protein dynamics, T_1 values and heteronuclear NOEs depend on internal motions occurring at high frequencies of 10^8–10^{12} s^{-1}, whereas T_2 values are also sensitive to much lower frequency motions (10^3–10^6 s^{-1}) (31). Plots of these relaxation parameters for H-RasT35S·GppNHp clearly showed that the regions comprising the residues 31–42, 61–75, 107–109, and 121–123 exhibit significant rapid internal motions on the picosecond to nanosecond time scale, *i.e.* lower values of T_1 and heteronuclear NOE in contrast to higher T_2 values (Fig. 5*A*). The backbone dynamics and structural orientations in the residues 107–109 (L7 loop between α3 and β5) and 121–123 (L8 loop between β5 and α4) were almost identical to those of H-Ras-GDP (data not shown) (30), indicating that the motions of these regions occur irrespective of the nucleotide type. Both switch I and switch II of state 1 were shown to be flexible as predicted from the x-ray analyses. This implied that the genuine mobilities, not the lack of experimental restraints, are the reason why the two switch regions are ill-defined in the solution structures of H-RasT35S·GppNHp. The relaxation data of H-RasT35S·GppNHp were drastically different from those of H-Ras·GppNHp, of which ^{15}N T_2 values in the switch regions are extremely short due to the slow internal motions on the millisecond time scale (19). Therefore, the mobilities of the switch regions of H-RasT35S·GppNHp are close to those of H-Ras-GDP rather than those of H-Ras·GppNHp. Nevertheless, it is likely that the chemical exchange contribution partially remains as the ^{15}N T_2 values of Asp-33, Ser-35, and Glu-37 are significantly shorter than those of the other residues (Fig. 5*A*).

Next we examined how binding to c-Raf-1 RBD affects the internal motions of H-Ras·GppNHp. In the presence of c-Raf-1 RBD, ^{15}N T_1, T_2, and heteronuclear NOE values for most of the residues in the P-loop and the switch regions reached near the average value (Fig. 5*B*). However, the ^{15}N T_2 values for Asp-30, Thr-35, and Tyr-40 in or near switch I and Gly-60 in switch II were significantly shorter than the average, suggesting that the exchange contribution was not completely excluded even in the presence of 1.2-fold excess of the effector.

DISCUSSION

Slow Conformational Dynamics of the State Transition and Rapid Internal Motions Inherent in Each State—In the backbone amide ^{1}H,^{15}N HSQC spectra of H-Ras·GppNHp, the measurements at 5 °C result in the generation of two new signals for several individual residues that are unobservable at 25 °C and induction of peak splitting for other several residues that yield single peaks at 25 °C. These phenomena are typical of a two-site chemical exchange with a temperature-dependent decrease in the exchange rate. In either case, the two resonance peaks coincide very well with the peaks of state 1 and state 2, which are separately identified by using H-RasT35S·GppNHp and the H-Ras·GppNHp·c-Raf-1 RBD complex, respectively. Moreover, the mean value of the intensity ratios of the split peaks is close to the equilibrium constant between state 1 and state 2. These results clearly indicate that the slow exchange process observed in ^{1}H and ^{15}N NMR of H-Ras·GppNHp does correspond to the interconversion between state 1 and state 2.

The spatial distribution of the dynamic residues indicates that the state transition involves global conformational rearrangement centered around the effector interface (Fig. 2*C*). Global conformational dynamics of the GTP-bound H-Ras in the millisecond time scale was previously suggested from the analysis of the backbone amide ^{15}N spin relaxation relaxation-compensated Carr-Purcell-Meiboom-Gill measurements (21), which identified Ser-17 in the P-loop, Gly-75 in switch II, and several residues in the other regions as the residues involved. Our study, which deals with the residues showing peak splitting in the backbone amide ^{1}H,^{15}N HSQC spectra, is capable of detecting particularly dynamic residues upon the state transition. First, we reveal the dynamics of the residues whose signals were previously unobservable: Gly-10, Gly-12, and Gly-13 in the P-loop, Val-29 in the switch I-flanking region, Gly-60 in switch II, and Ile-21 and Asp-54 in the structured regions. Furthermore, we extend our analysis to the residues whose amide protons, $^{1}H_N$, undergo the slow exchange process: Gly-15 in the P-loop, Thr-148 in the other loops, and Val-8, Gln-25, and Leu-79 in the rigidly structured regions. A chemical shift difference value between the split peaks, $\Delta\delta$, reflects a chemical environmental change upon the state transition. We observe notable differences in multiple residues, Gly-10, Gly-12, Gly-13, and Gly-15, in the P-loop in addition to the residues in the switch II loop and the regions flanking the switch I and switch II (Fig. 2*B*). This is rather unexpected because the P-loop does not display a significant conformational difference between the x-ray structures of H-RasT35S·GppNHp (state 1) and H-Ras·GppNHp (state 2) (data not shown) and because the backbone ^{15}N dynamics of this loop fails to show any conformational flexibility in both state 1 and state 2 (Fig. 5, *A* and *B*). We speculate that the large chemical shift differences of the P-loop residues may be caused by the effect of the conformational change of their neighboring regions such as switch II rather than their intrinsic conformational changes. Furthermore, we detect Gln-95 in the α3-helix as a residue showing peak splitting, suggesting that the α3-helix undergoes a conformational change upon the state transition. This is supported by the result of the ^{15}N spin relaxation relaxation-compensated Carr-Purcell-Meiboom-Gill measurements, showing that the residues 89–90, 93–96, and 98 in the α3-helix are involved in the slow dynamics (21). Because the α3-helix is also located adjacent to switch II, these residues may be sensitive to the conformational change of switch II. It was reported that certain amino acid substitutions in the P-loop (8) and the α3-helix (32) caused substantial shifts of the conformational equilibrium between state 1 and state 2, supporting our notion that both the P-loop and the α3-helix interact with switch II and facilitate the transition of state 1 to state 2.

Analysis of the backbone dynamics involving rapid internal motions of the GTP-bound H-Ras has been hampered by the existence of the slow conformational exchange process, namely the state transition. In this study the effect of the state transition is mostly excluded by using a T35S mutant and a complex with c-Raf-1 RBD for extraction of the dynamics intrinsic to state 1 and state 2, respectively. The ^{15}N T_1, T_2, and heteronuclear NOE values of H-RasT35S·GppNHp clearly show that the switch regions exhibit significant rapid internal motions on the picosecond to nanosecond time scale, which provide state 1 with further flexibility. It is intriguing that T35S replacement in switch I, which weakens interactions with the nucleotide (9, 13), makes both the switch regions flexible. On the other hand, the relaxation data of the H-Ras·GppNHp in complex with c-Raf-1 RBD indicate that most of the residues in the switch regions in state 2 are as rigid as the other structured regions of the protein. This result is supported from the state 2-specific conformational feature, in which guanine nucleotide-mediated interactions between switch I and switch II fix these regions (13). Consequently, the backbone dynamics of the two states suggest that the immobilization or folding of the two switch regions through these interactions is a cooperative process. Interestingly, another signaling protein, $NtrC^r$, has similar conformational features in its active and inactive states (33), *i.e.* multi-conformations exist in the inactive state, whereas these are mostly deselected upon activation, although $NtrC^r$ is activated by phosphorylation of its receiver domain. In the case of Ras, because the effector binding stabilizes state 2 and eliminates backbone conformations inherent in the highly mobile state 1 conformer, it would appear to have a large entropy cost in addition to the decrease in the rotational and translational entropy associated with binding of two protein molecules (34). This unfavorable entropy loss would be compensated mainly by a favorable enthalpy effect (35). Furthermore, the fast side-chain dynamics in Ras may also contribute to free energy of the effector binding (36). For example, other signaling proteins, calmodulin (37) and Cdc42Hs (38), reportedly undergo widespread redistributions in side-chain dynamics upon binding to their target proteins or peptides, suggesting the importance of

side-chain entropy in extensive regions centered around the protein-protein interfaces. Therefore, in addition to the dynamic behavior of the main chain in proteins, which is characterized in our experiments, residual conformational entropy arising from changes in the fast side-chain dynamics might be significantly connected to target binding of signaling proteins.

State 1-specific Conformation of the Switch Regions and Its Implication for Interaction with Sos—The solution structure of H-RasT35S·GppNHp faithfully reflects the state 1 conformation of H-Ras·GppNHp because its backbone $^{1}H,^{15}N$ cross-peaks coincide very well with the state 1 peaks of H-Ras·GppNHp. Although the backbone ^{15}N dynamics indicate similar internal motions of the switch regions in H-RasT35S·GppNHp and H-Ras-GDP, r.m.s.d. calculations based on their solution structures show the existence of significant differences. The switch II loop of H-Ras-GDP displays a wide range of backbone trajectories, whereas that of H-RasT35S·GppNHp is moderately constrained by some nonlocal interactions (Fig. 4*B*). In sharp contrast, the switch I loop of H-RasT35S·GppNHp exhibits a marked fluctuation compared with that of H-Ras-GDP. The large fluctuation resulting from the loss of the Thr-35-γ-phosphate interaction is supported by a structural study of H-Ras in state 1 using molecular dynamics simulations (39). Furthermore, some of the 20 backbone trajectories of switch I extend toward the structure of the nucleotide-free form in complex with Sos (Fig. 4*A*). X-ray structure analyses of the H-Ras-Sos complex showed the conformational features of the nucleotide-free H-Ras (16, 40); 1) the switch I loop is further pulled away from the nucleotide-binding site by the insertion of the helical hairpin segment of Sos, and 2) switch II is held very tightly by Sos, and large interfaces involving switch II are formed through numerous side-chain interactions in the complex.

We reason that the structural feature of H-RasT35S·GppNHp, capable of moving the switch I loop away from the nucleotide to an extent similar to that of the nucleotide-free form, may give an energetic advantage for stabilization of the H-Ras-Sos complex. To test our hypothesis, H-Ras/Sos binding was measured by *in vitro* binding assay and isothermal titration calorimetry using mSos1W729E possessing the intact guanine nucleotide exchange factor catalytic site, whereas its distal Ras-binding site is inactivated. As a result, H-RasT35S·GppNHp exhibits a stronger Sos binding activity than that of H-Ras·GppNHp (supplemental Fig. 2 and 3), supporting our hypothesis. However, its binding activity is weaker than that of H-Ras-GDP (supplemental Fig. 2 and 3), which appears to contradict the conformational similarity of the switch I loop with the nucleotide-free form. We speculate that this discrepancy may be accounted for by the difference in the mobility of the switch II loop, which is constrained presumably by the Gly-60-γ-phosphate interaction in H-RasT35S·GppNHp but not in H-Ras-GDP (Fig. 4, *B* and *C*). The structures of Ala-59 and Gln-61 neighboring Gly-60 are also significantly altered in H-RasT35S·GppNHp; the side chain of Ala-59 orients away from the nucleotide, whereas that of Gln-61 orients toward the nucleotide (Fig. 4*C*). The side-chain orientations of Ala-59 and Gln-61 in H-RasT35S·GppNHp include those of the corresponding residues in the state 2 structure of H-Ras·GppNHp and exhibit a nearly opposite orientation to those in the nucleotide-free H-Ras in the H-Ras-Sos complex (Fig. 4*C*). In contrast, the side-chain orientations of Ala-59 and Gln-61 of H-Ras-GDP include those similar to the nucleotide-free form. Thus, it is likely that the structural features of the switch II loop of H-RasT35S·GppNHp would make a substantial disadvantage for the interaction with Sos, accounting for its weaker binding activity to Sos than H-Ras-GDP.

In conclusion, our study has successfully determined the solution structure and dynamics of state 1 by NMR analysis of H-RasT35S·GppNHp, which faithfully reflects those of H-Ras·GppNHp as proved by the coincidence of the assigned signals between the two proteins. The structural information on state 1 of wild-type Ras, unveiled for the first time in this study, will provide an invaluable tool for the structure-based drug design of Ras inhibitors.

Acknowledgments—We gratefully acknowledge Takahisa Ikegami (Institute for Protein Research, Osaka University) for the residual dipolar coupling measurements and analyses and Tomoko Inoue for excellent technical assistance.

REFERENCES

1. Vetter, I. R., and Wittinghofer, A. (2001) *Science* **294,** 1299–1304
2. Corbett, K. D., and Alber, T. (2001) *Trends Biochem. Sci.* **26,** 710–716
3. Downward, J. (2003) *Nat. Rev. Cancer* **3,** 11–22
4. Spoerner, M., Hozsa, C., Poetzl, J. A., Reiss, K., Ganser, P., Geyer, M., and Kalbitzer, H. R. (2010) *J. Biol. Chem.* **285,** 39768–39778
5. Geyer, M., Schweins, T., Herrmann, C., Prisner, T., Wittinghofer, A., and Kalbitzer, H. R. (1996) *Biochemistry* **35,** 10308–10320
6. Spoerner, M., Nuehs, A., Herrmann, C., Steiner, G., and Kalbitzer, H. R. (2007) *FEBS J.* **274,** 1419–1433
7. Liao, J., Shima, F., Araki, M., Ye, M., Muraoka, S., Sugimoto, T., Kawamura, M., Yamamoto, N., Tamura, A., and Kataoka, T. (2008) *Biochem. Biophys. Res. Commun.* **369,** 327–332
8. Spoerner, M., Wittinghofer, A., and Kalbitzer, H. R. (2004) *FEBS Lett.* **578,** 305–310
9. Spoerner, M., Herrmann, C., Vetter, I. R., Kalbitzer, H. R., and Wittinghofer, A. (2001) *Proc. Natl. Acad. Sci. U.S.A.* **98,** 4944–4949
10. Pai, E. F., Krengel, U., Petsko, G. A., Goody, R. S., Kabsch, W., and Wittinghofer, A. (1990) *EMBO J.* **9,** 2351–2359
11. Huang, L., Hofer, F., Martin, G. S., and Kim, S. H. (1998) *Nat. Struct. Biol.* **5,** 422–426
12. Pacold, M. E., Suire, S., Perisic, O., Lara-Gonzalez, S., Davis, C. T., Walker, E. H., Hawkins, P. T., Stephens, L., Eccleston, J. F., and Williams, R. L. (2000) *Cell* **103,** 931–943
13. Shima, F., Ijiri, Y., Muraoka, S., Liao, J., Ye, M., Araki, M., Matsumoto, K., Yamamoto, N., Sugimoto, T., Yoshikawa, Y., Kumasaka, T., Yamamoto, M., Tamura, A., and Kataoka, T. (2010) *J. Biol. Chem.* **285,** 22696–22705
14. Ford, B., Skowronek, K., Boykevisch, S., Bar-Sagi, D., and Nassar, N. (2005) *J. Biol. Chem.* **280,** 25697–25705
15. Ye, M., Shima, F., Muraoka, S., Liao, J., Okamoto, H., Yamamoto, M., Tamura, A., Yagi, N., Ueki, T., and Kataoka, T. (2005) *J. Biol. Chem.* **280,** 31267–31275
16. Boriack-Sjodin, P. A., Margarit, S. M., Bar-Sagi, D., and Kuriyan, J. (1998) *Nature* **394,** 337–343
17. Kalbitzer, H. R., Spoerner, M., Ganser, P., Hozsa, C., and Kremer, W. (2009) *J. Am. Chem. Soc.* **131,** 16714–16719
18. Hu, J. S., and Redfield, A. G. (1997) *Biochemistry* **36,** 5045–5052
19. Ito, Y., Yamasaki, K., Iwahara, J., Terada, T., Kamiya, A., Shirouzu, M., Muto, Y., Kawai, G., Yokoyama, S., Laue, E. D., Wälchli, M., Shibata, T., Nishimura, S., and Miyazawa, T. (1997) *Biochemistry* **36,** 9109–9119
20. Fenwick, R. B., Prasannan, S., Campbell, L. J., Nietlispach, D., Evetts, K. A.,

Camonis, J., Mott, H. R., and Owen, D. (2009) *Biochemistry* **48,** 2192–2206
21. O'Connor, C., and Kovrigin, E. L. (2008) *Biochemistry* **47,** 10244–10246
22. Gill, S. C., and von Hippel, P. H. (1989) *Anal. Biochem.* **182,** 319–326
23. Cavanagh, J., Fairbrother, W. J., Skelton, N. J., and Palmer, A. G. (1996) *Protein NMR Spectroscopy*, Academic Press, San Diego, CA
24. Farrow, N. A., Muhandiram, R., Singer, A. U., Pascal, S. M., Kay, C. M., Gish, G., Shoelson, S. E., Pawson, T., Forman-Kay, J. D., and Kay, L. E. (1994) *Biochemistry* **33,** 5984–6003
25. Kay, L. E., Nicholson, L. K., Delaglio, F., Bax, A., and Torchia, D. A. (1992) *J. Magn. Reson.* **97,** 359–375
26. Güntert, P., Mumenthaler, C., and Wüthrich, K. (1997) *J. Mol. Biol.* **273,** 283–298
27. Brünger, A. T., Adams, P. D., Clore, G. M., DeLano, W. L., Gros, P., Grosse-Kunstleve, R. W., Jiang, J. S., Kuszewski, J., Nilges, M., Pannu, N. S., Read, R. J., Rice, L. M., Simonson, T., and Warren, G. L. (1998) *Acta Crystallogr. D Biol. Crystallogr.* **54,** 905–921
28. Cornilescu, G., Delaglio, F., and Bax, A. (1999) *J. Biomol. NMR* **13,** 289–302
29. Laskowski, R. A., Rullmannn, J. A., MacArthur, M. W., Kaptein, R., and Thornton, J. M. (1996) *J. Biomol. NMR* **8,** 477–486
30. Kraulis, P. J., Domaille, P. J., Campbell-Burk, S. L., Van Aken, T., and Laue, E. D. (1994) *Biochemistry* **33,** 3515–3531
31. Kay, L. E., Torchia, D. A., and Bax, A. (1989) *Biochemistry* **28,** 8972–8979
32. Matsumoto, K., Shima, F., Muraoka, S., Araki, M., Hu, L., Ijiri, Y., Hirai, R., Liao, J., Yoshioka, T., Kumasaka, T., Yamamoto, M., Tamura, A., and Kataoka, T. (2011) *J. Biol. Chem.* **286,** 15403–15412
33. Kern, D., Volkman, B. F., Luginbühl, P., Nohaile, M. J., Kustu, S., and Wemmer, D. E. (1999) *Nature* **402,** 894–898
34. Tamura, A., and Privalov, P. L. (1997) *J. Mol. Biol.* **273,** 1048–1060
35. Wohlgemuth, S., Kiel, C., Krämer, A., Serrano, L., Wittinghofer, F., and Herrmann, C. (2005) *J. Mol. Biol.* **348,** 741–758
36. Wand, A. J. (2001) *Nat. Struct. Biol.* **8,** 926–931
37. Lee, A. L., Kinnear, S. A., and Wand, A. J. (2000) *Nat. Struct. Biol.* **7,** 72–77
38. Loh, A. P., Pawley, N., Nicholson, L. K., and Oswald, R. E. (2001) *Biochemistry* **40,** 4590–4600
39. Kobayashi, C., and Saito, S. (2010) *Biophys. J.* **99,** 3726–3734
40. Cherfils, J., and Chardin, P. (1999) *Trends Biochem. Sci.* **24,** 306–311
41. Koradi, R., Billeter, M., and Wüthrich, K. (1996) *J. Mol. Graph.* **14,** 51–55, 29–32

THE JOURNAL OF BIOLOGICAL CHEMISTRY VOL. 286, NO. 17, pp. 15403–15412, April 29, 2011

Critical Roles of Interactions among Switch I-preceding Residues and between Switch II and Its Neighboring α-Helix in Conformational Dynamics of the GTP-bound Ras Family Small GTPases*[S]

Received for publication, November 19, 2010, and in revised form, February 21, 2011 Published, JBC Papers in Press, March 9, 2011, DOI 10.1074/jbc.M110.204933

Kousuke Matsumoto[‡1], Fumi Shima[‡1], Shin Muraoka[‡§1], Mitsugu Araki[¶], Lizhi Hu[‡], Yuichi Ijiri[‡], Rina Hirai[‡], Jingling Liao[‡], Takashi Yoshioka[¶], Takashi Kumasaka[‖], Masaki Yamamoto[§], Atsuo Tamura[¶], and Tohru Kataoka[‡2]

From the [‡]Division of Molecular Biology, Department of Biochemistry and Molecular Biology, Kobe University Graduate School of Medicine, 7-5-1 Kusunoki-cho, Chuo-ku, Kobe 650-0017, the [¶]Department of Chemistry, Kobe University Graduate School of Science, 1-1 Rokkodai, Nada-ku, Kobe 657-8501, the [‖]Japan Synchrotron Radiation Research Institute (JASRI), 1-1-1 Kouto, Sayo-cho, Sayo-gun, Hyogo 679-5198, and the [§]RIKEN SPring-8 Center, 1-1-1 Kouto, Sayo-cho, Sayo-gun, Hyogo 679-5148, Japan

GTP-bound forms of Ras family small GTPases exhibit dynamic equilibrium between two interconverting conformations, "inactive" state 1 and "active" state 2. A great variation exists in their state distribution; H-Ras mainly adopts state 2, whereas M-Ras predominantly adopts state 1. Our previous studies based on comparison of crystal structures representing state 1 and state 2 revealed the importance of the hydrogen-bonding interactions of two flexible effector-interacting regions, switch I and switch II, with the γ-phosphate of GTP in establishing state 2 conformation. However, failure to obtain both state structures from a single protein hampered further analysis of state transition mechanisms. Here, we succeed in solving two crystal structures corresponding to state 1 and state 2 from a single Ras polypeptide, M-RasD41E, carrying an H-Ras-type substitution in residue 41, immediately preceding switch I, in complex with guanosine 5′-(β,γ-imido)triphosphate. Comparison among the two structures and other state 1 and state 2 structures of H-Ras/M-Ras reveal two new structural features playing critical roles in state dynamics; interaction of residues 31/41 (H-Ras/M-Ras) with residues 29/39 and 30/40, which induces a conformational change of switch I favoring its interaction with the γ-phosphate, and the hydrogen-bonding interaction of switch II with its neighboring α-helix, α3-helix, which induces a conformational change of switch II favoring its interaction with the γ-phosphate. The importance of the latter interaction is proved by mutational analyses of the residues involved in hydrogen bonding. These results define the two novel functional regions playing critical roles during state transition.

H-Ras, K-Ras, and N-Ras, collectively called Ras, are the products of the *ras* proto-oncogenes and belong to the Ras family of small GTPases, which also includes Rap1, Rap2, R-Ras, R-Ras2/TC1, M-Ras/R-Ras3, Ral etc. (1, 2). They function as guanine nucleotide-dependent molecular switches by cycling between the GTP-bound active and GDP-bound inactive forms in intracellular signaling pathways controlling cell growth and differentiation (3). The interconversion between the GDP-bound and GTP-bound forms is catalyzed by guanine nucleotide exchange factors and GTPase-activating proteins (4, 5). X-ray crystallographic and NMR analyses of H-Ras and Rap1A, alone or in complex with their effectors, revealed that the exchange of GTP for GDP results in allosteric conformational changes in two adjacent regions, termed switch I (residues 32–38) and switch II (residues 60–75), consisting of a single loop and a loop and an α-helix (α2-helix), respectively, and enables Ras to execute downstream signaling through direct interaction with its effectors, such as Raf kinases, phosphoinositide 3-kinases, and phospholipase Cε (3, 4) (see supplemental Fig. S1). Switch I almost overlaps with the effector region (residues 32–40), which forms a principal binding interface for effector recognition (6–9).

^{31}P NMR studies revealed that H-Ras and K-Ras in complex with Mg^{2+} and a non-hydrolyzable GTP analog, GppNHp,[3] exhibit equilibrium between the two conformational states, termed state 1 and state 2 (10). The two states are characterized by different chemical shift values for the resonances of the phosphorous atoms of the α- and γ-phosphate groups of GppNHp. The chemical shift values are mainly influenced by the distance of the phosphate groups from the aromatic ring of Tyr-32 in switch I, which exerts a "ring current shift" effect (10). The interconversion between the two states occurs in a millisecond time scale and appears to be a general property shared by members of the Ras family small GTPases irrespective of the nature of the bound guanine nucleotide triphosphate: GTP, GppNHp, or GTPγS (10–13). However, the state distribution exhibited a great variation even among closely related GTPase species; the state 1 population occupies 36 ± 2, 15 ± 1, and 93 ± 2% for H-Ras, Rap1A, and M-Ras, respectively (12), which pos-

* This work was supported by Grants-in-aid for Scientific Research in Priority Areas 17014061 and 18057014, and Global COE Program A08 from the Ministry of Education, Science, Sports and Culture of Japan, and by a grant from the Program for Promotion of Fundamental Studies of Health Sciences 06-3 from the National Institute of Biomedical Innovation.

[S] The on-line version of this article (available at http://www.jbc.org) contains supplemental Tables S1 and S2 and Figs. S1–S7.

[1] These authors contributed equally to this work.

[2] To whom correspondence should be addressed. Tel.: 81-78-382-5380; Fax: 81-78-382-5399; E-mail: kataoka@people.kobe-u.ac.jp.

[3] The abbreviations used are: GppNHp, guanosine 5′-(β,γ-imido)triphosphate; GTPγS, guanosine 5′-3-*O*-(thio)triphosphate; RBD, Ras-binding domain.

sess the identical switch I residues and share some of the effectors such as c-Raf-1 (14, 15). Because association of H-Ras-GppNHp with its effectors such as c-Raf-1 induced a shift of the equilibrium toward state 2, state 1 and state 2 were presumed to represent inactive and active conformations, respectively (10).

Although the crystal structures corresponding to state 2 had been solved with H-Ras-GppNHp alone or in complex with the effectors (8, 9, 16, 17), those corresponding to state 1 remained unsolved until our determination of the crystal structure of M-Ras-GppNHp (18). So far, state 1 structures were solved with the crystals of the GppNHp-bound forms of M-Ras (18), H-RasG60A (19), H-RasG60A/K147A (20), M-RasP40D (21), and H-RasT35S (21). H-RasT35S yielded two distinct structures, termed form 1 and form 2. Comparison of these structures with state 2 structures indicated that the most fundamental feature distinguishing state 1 from state 2 is the loss of the direct and Mg^{2+}-coordinated indirect hydrogen-bonding interactions of Thr-35/45 (H-Ras/M-Ras) in switch I with the γ-phosphate of GppNHp. This results is in marked deviation of the switch I loop away from the guanine nucleotide and increases the distance between Tyr-32/42 and the γ-phosphate, accounting for at least a major part of the observed ^{31}P NMR chemical shift changes. Moreover, the structures of M-Ras-GppNHp and H-RasT35S-GppNHp form 1 revealed another key structural feature of state 1, the loss of the hydrogen-bonding interaction between Gly-60/70 in switch II and the γ-phosphate, whose importance was also supported by the adoption of the state 1 conformation by H-RasG60A-GppNHp and H-RasG60A/K147A-GppNHp (19, 20). Thus, the state 2 structure is characterized by stabilization of the switch I and switch II loops to the nucleotide through interactions of Thr-35/45 and Gly-60/70 with the γ-phosphate. The results also indicated the importance of the nucleotide-mediated interdependence between the two switch regions because a mutation in one switch region induced a gross conformational change of the other switch region (19–21). The structures of M-RasP40D-GppNHp and H-RasT35S-GppNHp form 2, retaining the Gly-60/70-γ-phosphate interaction whereas losing the Thr-35/45-γ-phosphate interaction, were presumed to represent the intermediate between the two states (21). However, these analyses were carried out by comparison of the crystal structures representing either state derived from different mutant polypeptides, which tended to be compromised by the secondary effects of the mutations. Thus, further analysis of the state transition mechanisms needed determination of both state structures from a single Ras polypeptide.

In the present study, we utilize the M-RasD41E polypeptide to solve both state 1 and state 2 crystal structures in the GppNHp-bound forms. The D41E mutation, where Asp-41 of M-Ras was substituted by the corresponding Glu-31 of H-Ras, was known to increase state 1 occupancy of M-Ras most efficiently as a single mutation from our previous study (21). Comparison of the resulting two crystal structures corresponding to state 1 and state 2 reveal two new structural features pertaining to the state transition; the interaction among the residues immediately preceding switch I including Glu-31/Asp-41 and the hydrogen-bonding interaction of switch II with the α3-helix. The two interactions facilitate establishment of the Thr-35/45-γ-phosphate and Gly-60/70-γ-phosphate interactions, respectively, and thereby induce the shift of state equilibrium toward state 2. Applicability of this mechanism to other members of the Ras family small GTPases, H-Ras, and more distantly related RalA, will be discussed.

EXPERIMENTAL PROCEDURES

Protein Purification—Mouse M-RasD41E (residues 1–178) was expressed as fusions with glutathione *S*-transferase in *Escherichia coli* BL21(DE3) using pGEX-6P-1 vector (GE Healthcare, Buckinghamshire, UK), immobilized on glutathione-agarose, and eluted by cleavage with PreScission protease (GE Healthcare). After further purification by ion exchange chromatography to the final purity of >95%, it was loaded with GppNHp and used for crystallization or NMR spectroscopy as described before (18). Human c-Raf-1 RBD (residues 51–130) was purified as described (12).

NMR Spectroscopy—^{31}P NMR spectra were recorded in the presence or absence of c-Raf-1 RBD on a Brucker AVANCE-500 NMR spectrometer (18). The ^{31}P spectra were referenced as described (22).

Crystallization of Ras Proteins in Complex with Mg^{2+} and GppNHp—M-RasD41E-GppNHp was dissolved in buffer (50 mM Tris-HCl, pH 7.4, 50 mM NaCl, 5 mM $MgCl_2$, and 1 mM DTT). Crystals of M-RasD41E-GppNHp were grown by the sitting drop vapor diffusion method at 20 °C in drops containing 1 μl of protein solution (19 mg/ml) and 1 μl of reservoir 1 (100 mM Tris-HCl, pH 8.5, 200 mM $MgCl_2$, and 20% (w/v) PEG 8000) for 1 week, or in drops containing 0.8 μl of protein solution 2 (21.5 mg/ml) and 1 μl of reservoir 2 (100 mM Tris-HCl, pH 6.5, 200 mM $MgCl_2$, and 25% (w/v) PEG 8000) for 3 weeks, respectively. Crystals with space group $P622$ grew in reservoir 1, whereas those with space group $P2_12_12_1$ grew in reservoir 2.

Data Collection and Structure Determination—The data collections at 100 K were carried out at BL38B1 using Jupiter 210 (Rigaku corporation) or Quantum 210 (ADSC) CCD detectors in SPring-8. Distinct structures, type 1 and type 2, were solved from the crystals with space groups $P622$ and $P2_12_12_1$, respectively. The data for M-RasD41E-GppNHp type 1 were processed using the program HKL2000 (23), whereas those for type 2 were processed with the program MOSFLM (24) and scaled with the program SCALA in the CCP4 program suite (25). The crystal structures were determined by the molecular replacement method with MOLREP (26) using M-Ras-GppNHp (Protein Data Bank code 1X1S) as a search model. After the two models were refined with programs CNS (27) and REFMAC (28), their stereochemical quality was checked with PROCHECK in the CCP4 program suit (29). The data collection and refinement statistics are summarized in supplemental Table S1. The number of detected water molecules in type 1 (resolution = 2.75 Å) was substantially smaller than that in type 2 (resolution = 1.55 Å). Thus, the assignment of water-mediated hydrogen bonds in type 1 was done with great care only in reference to those found in type 2, when the corresponding water molecules were invisible.

Graphics—The figures were prepared with PyMOL (DeLano Scientific).

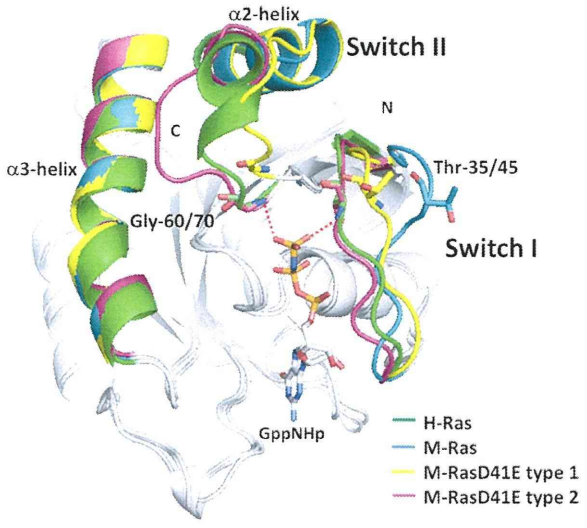

FIGURE 1. **Comparison of the crystal structures of M-RasD41E-GppNHp types 1 and 2 with those of M-Ras-GppNHp and H-Ras-GppNHp with a special emphasis on switch I, switch II, and the α3-helix.** Superimposition of the backbone structures of M-Ras-GppNHp, M-RasD41E-GppNHp type 1, M-RasD41E-GppNHp type 2, and H-Ras-GppNHp. Only switch I, switch II, and the α3-helix are colored as indicated. The structure of GppNHp is excerpted from the model of M-RasD41E-GppNHp type 2. GppNHp and the side chains of Thr-35/45 and Gly-60/70 (H-Ras/M-Ras) are shown in the *stick model* (*red*, oxygen; *blue*, *nitrogen*; *deep pink*, phosphorus). Direct hydrogen bonds of Thr-45 and Gly-70 with the γ-phosphate in type 2 are shown by *red dotted lines*, whereas Mg^{2+}- or water-mediated hydrogen bonds (see supplemental Fig. 2) are not shown. The models were generated with PyMOL, based on the least square fittings of the Cα atoms of the residues excluding those of the two switch regions.

PDB Codes of the Coordinates Used in this Paper—M-RasD41E-GppNHp type 1, PDB code 3PIR; M-RasD41E-GppNHp type 2, PDB code 3PIT; M-Ras-GppNHp, PDB code 1X1S; M-RasP40D-GppNHp, PDB code 3KKP; M-RasP40D/D41E/L51R-GppNHp, PDB code 3KKO; H-Ras-GppNHp, PDB code 1CTQ; H-RasT35S-GppNHp form 2, PDB code 3KKM; Rap2A-GTP, PDB code 3RAP chain R; RalA-GppNHp, PDB code 1U8Y chain B were used.

RESULTS

Determination of Two Distinct Crystal Structures of M-RasD41E-GppNHp, Corresponding to State 1 and State 2—We previously showed that the residues immediately preceding switch I (hereafter termed pre-switch I residues) of M-Ras (supplemental Fig. S1), particularly Pro-40 and Asp-41, play critical roles in its state 1 predominance because H-Ras-type substitutions for these residues, P40D and D41E, caused a significant increase in the state 2 population (21). In particular, M-RasD41E-GppNHp exhibited the most prominent increase of the state 2 population to 21 ± 2 over 7 ± 2% of M-Ras-GppNHp (supplemental Table S2). This led us to examine crystallization conditions of M-RasD41E-GppNHp for crystals representing either state. With the use of two distinct conditions different in pH and PEG8000 concentrations (see "Experimental Procedures"), we obtained two crystals with a different space group, which yielded two distinct tertiary structures, type 1 and type 2 (supplemental Table S1). Their overall structures superimposed very well with those of M-Ras-GppNHp and H-Ras-GppNHp, representing state 1 and state 2 structures, respectively, except the two switch regions (Fig. 1). Electron density of residues 69–73 in switch II, which were invisible in the M-Ras-GppNHp structure (18), was completely clear in both structures. The effect of crystal packing on the determined structures seemed negligible. Although we observed dot-like contacts only at residues 74 and 112 with a neighboring molecule in type 1, such extremely faint contacts were unlikely to affect the conformation of the corresponding regions. Indeed, the temperature factor values for the two residues were kept high, suggesting that these residues were not fixed by crystal packing.

M-RasD41E-GppNHp type 1 exhibited the loss of the interactions of both Thr-45 in switch I and Gly-70 in switch II with the γ-phosphate of GppNHp (see also supplemental Fig. S2) and deviation of the switch I loop away from the nucleotide, indicating that it corresponded to state 1. Indeed, switch II residues of type 1 superimposed very well with the visible part of switch II residues of M-Ras-GppNHp (Fig. 1) and the type 1 crystal possessed similar unit cell dimensions and the same space group with the M-Ras-GppNHp crystal, implying similar crystal packing. Although no interaction was recognized between the switch I loop and γ-phosphate, Thr-45 of type 1 showed a significant positional shift approaching the γ-phosphate compared with that of M-Ras-GppNHp and was located in the middle positions of Thr-45 of M-Ras-GppNHp (state 1) and Thr-35 of H-Ras-GppNHp (state 2) (Fig. 1). This positional change of Thr-45 of type 1 may facilitate establishment of a hydrogen-bonding interaction with the γ-phosphate and account for the increase of the state 2 population in M-RasD41E-GppNHp.

On the other hand, M-RasD41E-GppNHp type 2 corresponded to state 2 because the interactions of both Thr-45 and Gly-70 with the γ-phosphate were retained as commonly observed in state 2 conformers such as H-Ras-GppNHp and M-RasP40D/D41E/L51R (21) (Fig. 1 and supplemental Figs. S2 and S3). Indeed, the backbone structures of the switch I loop and α2-helix in switch II of type 2 superimposed very well with those of state 2 conformers, except switch II loop residues, which exhibited a minor conformational change (Fig. 1 and supplemental Fig. S3). Thus, M-RasD41E-GppNHp yielded both state 1 and state 2 crystal structures for the first time as Ras family small GTPases.

Structural Differences Around Switch I and Switch II between Type 1 and Type 2—We made a detailed comparison of the structures of the switch I and switch II regions, which exhibited marked differences between M-RasD41E-GppNHp type 1 and type 2 (Fig. 1). Because of the relatively low resolution of type 1, we predicted the existence of water-mediated hydrogen bonds in type 1 only for those actually detected in type 2 when the corresponding water molecules were invisible.

Comparison of the structures of the switch I and pre-switch I regions indicated that Tyr-42 exhibited the most drastic positional changes (Fig. 2). In type 2, where the Thr-45-γ-phosphate hydrogen-bonding interaction was present, the side chain of Tyr-42 was located very close to the nucleotide (Fig. 2*A*). In contrast, it was pulled far away from the nucleotide in type 1, which lacked the Thr-45-γ-phosphate interaction (Fig. 2*B*). Consistent with this, the main chain amide of the adjacent

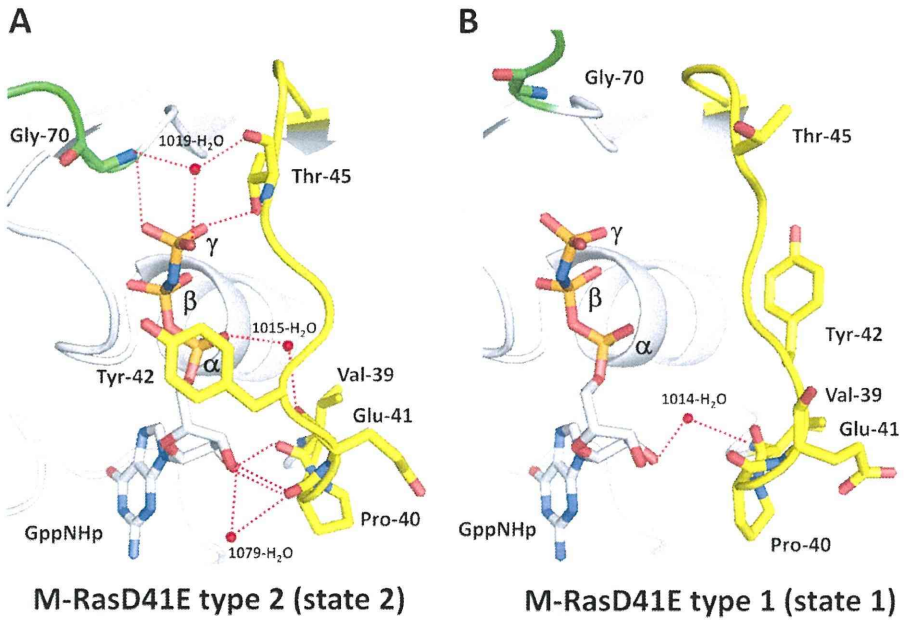

FIGURE 2. **Comparison of the hydrogen-bonding networks around the pre-switch I and switch I regions between M-RasD41E-GppNHp types 1 and 2.** The pre-switch I and switch I residues (*yellow*) and the switch II residue Gly-70 (*green*) are shown for M-RasD41E-GppNHp type 2 (*A*) and type 1 (*B*). Oxygen (*red*) and nitrogen (*blue*) atoms are shown only for the main chains and side chains of Val-39, Pro-40, Glu-41, Tyr-42, Thr-45, and Gly-70, and GppNHp. Water molecules mediating hydrogen bonds are shown by *red balls*, whereas hydrogen bonds are shown by *red dotted lines*. The models were generated with PyMOL.

Glu-41 formed a water-mediated hydrogen bond with the α-phosphate of GppNHp in type 2, whereas the corresponding interaction was absent in type 1 (Fig. 2 and supplemental Fig. S2). Moreover, the modes of interaction with the ribose ring of GppNHp showed a marked difference; Val-39 formed a direct hydrogen bond and Pro-40 formed both direct and water-mediated hydrogen bonds in type 2, whereas type 1 formed only a water-mediated hydrogen bond via Val-39. Thus, the hydrogen-bonding network in switch I and the pre-switch I regions of type 2 showed closer resemblance to that of H-Ras-GppNHp than that of M-Ras-GppNHp (supplemental Fig. S2). These results hinted at an intimate relationship of the composition of the hydrogen-bonding networks in these regions with the formation of the Thr-45/35-γ-phosphate (M-Ras/H-Ras) hydrogen bond, the determinant of the conformational states. Mechanisms underlying this relationship will be discussed (see "Discussion").

Comparison of the structures of the switch II region indicated that α2-helix was located close to the α3-helix in type 2 compared with that in type 1 (Fig. 1). We observed a clear difference in the mode of interaction between switch II and the α3-helix. In type 2, where the Gly-70-γ-phosphate interaction was present, Glu-72, Glu-73, and Phe-74 in switch II formed direct and/or water-mediated hydrogen bonds with Arg-105 in the α3-helix (Fig. 3*A*). In sharp contrast, residues 70–79 including these 3 residues in switch II failed to form any hydrogen bonds with residues 105–109 in the α3-helix (Fig. 3*B*). Intriguingly, H-Ras-GppNHp exhibited hydrogen-bonding interactions between corresponding residues 60–69 in switch II and residues 95–99 in the α3-helix, which were similar to those observed in type 2 (Fig. 3*C*). However, the interactions were more intensive in the case of H-Ras-GppNHp; they were composed of a direct hydrogen bond of Asp-69 with Gln-99, and water-mediated hydrogen bonds of Arg-68 with Gln-95, Tyr-96, and Gln-99, and Gly-60 with Tyr-96. The α2-helices of type 2 and H-Ras-GppNHp exhibited a similar rotational change compared with that of type 1, and their Gly-70/60 (M-Ras/H-Ras) formed hydrogen bonds with the γ-phosphate of GppNHp (21) (Fig. 3, *A* and *C*).

Crucial Role of the Switch II-α3-Helix Interaction in Facilitating Adoption of State 2—The results described above suggested that the mode of the switch II-α3-helix interaction, which depends on the nature of the relevant residues, may play a critical role in state transition. Comparison of amino acid sequences showed that some of the residues involved in the switch II-α3-helix interactions were not conserved between H-Ras and M-Ras, such as Tyr-64 *versus* Phe-74 and Asp-69 *versus* Glu-79, respectively, in switch II, and Gln-95 *versus* Arg-105, Tyr-96 *versus* Phe-106, Glu-98 *versus* Gln-108, and Gln-99 *versus* Leu-109, respectively, in the α3-helix (supplemental Fig. S1). We knew from our previous study (21) that H-Ras-type amino acid substitutions for Phe-74 and Glu-79, F74Y and E79D, in M-Ras, alone or in combination with the P40D/D41E/L51R mutation (see supplemental Table S2), had no significant effect on state distribution. Accordingly, we introduced H-Ras-type amino acid substitutions for Arg-105, Phe-106, and Leu-109, *i.e.* R105Q, F106Y, and L109Q, into M-RasP40D/D41E/L51R/F74Y/E79D, and the resulting mutant polypeptides in complex with GppNHp were examined for the state distribution by ^{31}P NMR spectroscopy (Fig. 4). We used M-RasP40D/D41E/L51R/F74Y/E79D as the prototype for mutation because it possessed the hydrogen-bonding partner residues such as Tyr-74 and Asp-79 in switch II. The result clearly showed that only the L109Q substitution caused a substantial increase in the state 2 population; the state 2 peak of the γ-phosphate resonance line at −3.7 ppm increased to 47 ± 2% in M-RasP40D/

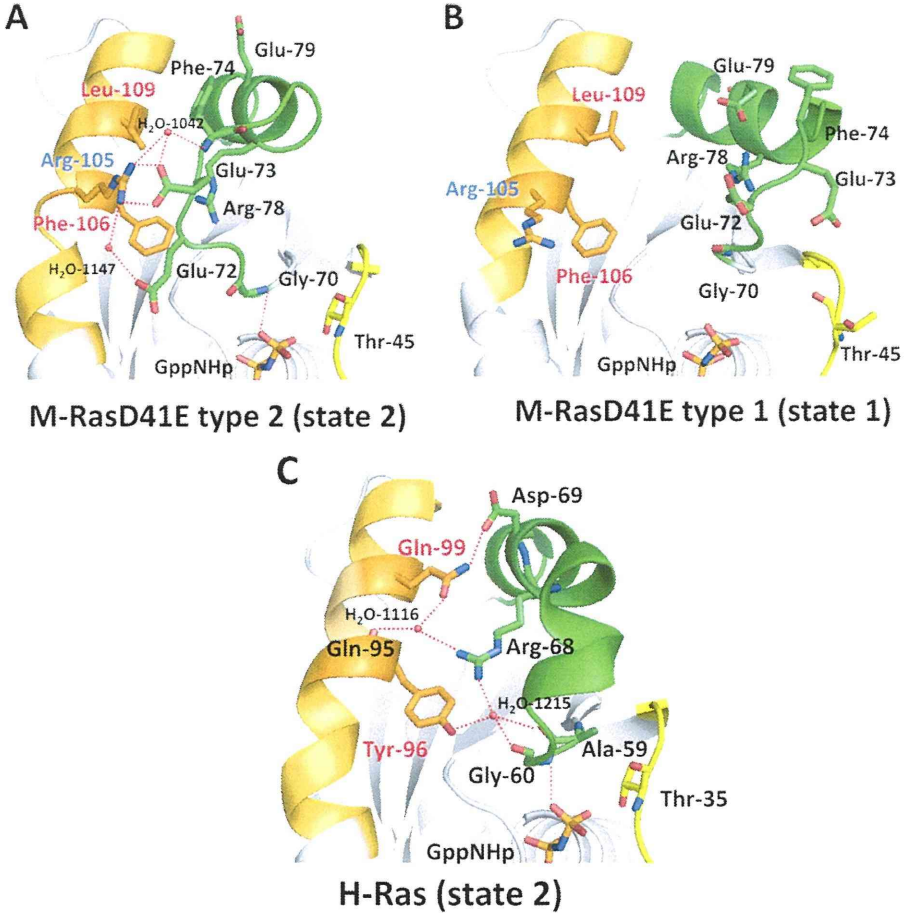

FIGURE 3. **Comparison of the hydrogen-bonding interactions between switch II and the α3-helix among M-RasD41E-GppNHp types 1 and 2 and H-Ras-GppNHp.** The tertiary structures around switch II and the α3-helices are shown for M-RasD41E-GppNHp type 2 (*A*), M-RasD41E-GppNHp type 1 (*B*), and H-Ras-GppNHp type 2 (*C*). Switch I, switch II, and the α3-helix are shown in *yellow*, *green*, and *orange*, respectively. Hydrogen bonds are shown by *red dotted lines*. The models were generated as described in the legend to Fig. 2.

D41E/L51R/F74Y/E79D/L109Q-GppNHp compared with 23 ± 3% at −3.68 ppm in M-RasP40D/D41E/L51R/F74Y/E79D-GppNHp (Fig. 4*B* and supplemental Table S2). The state assignment of the two peaks of the γ-phosphate resonance line for M-RasP40D/D41E/L51R/F74Y/E79D/L109Q-GppNHp was confirmed by addition of c-Raf-1 RBD (supplemental Fig. S3 and Table S2). The results suggested that restoration of the hydrogen-bonding interaction between Gln-109 and Asp-79, corresponding to the Gln-99—Asp-69 interaction in H-Ras, facilitated the adoption of state 2 in this M-Ras mutant. Collectively, our results implied that the higher density or proper arrangement of the hydrogen-bonding network between switch II and the α3-helix facilitates the adoption of state 2, resulting in the higher state 2 population.

Another H-Ras-type substitution, F106Y, in the α3-helix of M-RasP40D/D41E/L51R/F74Y/E79D, whether introduced alone or in combination with L109Y, caused a significant decrease in state 2 population even though the hydrogen-bonding partners of Tyr-106, Gly-70, and Arg-78 existed (Fig. 4, *A* and *B*). This unexpected effect of the F106Y substitution may be accounted for by the notion that the addition of a hydroxyl group to Phe-106 of M-RasD41E-GppNHp type 2 is likely to bring collision with the side chain of Asp-21 in the P-loop according to the calculation using the program PyMOL (supplemental Fig. S5). In the case of H-Ras-GppNHp, the less massive side chain of Ala-11, corresponding to Asp-21 of M-Ras, leads to an escape from the collision with Tyr-96. This finding suggests that the α3-helix-P-loop interaction may have a role in state transition.

DISCUSSION

Comparison of the Pre-switch I and Switch I Structures and Its Implication in the State Transition Mechanism of M-Ras—The positional change of Thr-45 of M-RasD41E-GppNHp type 1 approaching the nucleotide (Fig. 1) has prompted us to clarify its underlying mechanism focusing on the role of residue 41 on the switch I conformational changes during the state transition of M-Ras. To this end, we make a detailed comparison of the structures of the pre-switch I (residues 39–41) (Fig. 5) and switch I (residues 42–48) regions (Figs. 5 and 6) among M-Ras-GppNHp (state 1) and M-RasD41E-GppNHp types 1 (state 1) and 2 (state 2).

The configuration of residue 41 exhibits a clear difference among the three structures (Fig. 5, *A*-*C*). In M-RasD41E-